Hindawi Publishing Corporation
International Journal of Antennas and Propagation
Volume 2014, Article ID 984102, 12 pages
http://dx.doi.org/10.1155/2014/984102

Research Article

Fading Evaluation in the 60 GHz Band in Line-of-Sight Conditions

J. Reig,[1] M.-T. Martínez-Inglés,[2] L. Rubio,[1] V.-M. Rodrigo-Peñarrocha,[1] and J.-M. Molina-García-Pardo[2]

[1] *Grupo de Radiación Electromagnética (GRE), Universitat Politècnica de València, Camino de Vera s/n, 46022 Valencia, Spain*
[2] *Grupo de Sistemas de Comunicaciones Móviles (SiCoMo), Universidad Politécnica de Cartagena, Antigones, 30202 Cartagena, Spain*

Correspondence should be addressed to J. Reig; jreigp@dcom.upv.es

Received 9 May 2014; Revised 10 July 2014; Accepted 10 July 2014; Published 7 August 2014

Academic Editor: Jose F. Paris

An exhaustive analysis of the small-scale fading amplitude in the 60 GHz band is addressed for line-of-sight conditions (LOS). From a measurement campaign carried out in a laboratory, we have estimated the distribution of the small-scale fading amplitude over a bandwidth of 9 GHz. From the measured data, we have estimated the parameters of the Rayleigh, Rice, Nakagami-m, Weibull, and α-μ distributions for the small-scale amplitudes. The test of Kolmogorov-Smirnov (K-S) for each frequency bin is used to evaluate the performance of such statistical distributions. Moreover, the distributions of the main estimated parameters for such distributions are calculated and approximated for lognormal statistics in some cases. The matching of the above distributions to the experimental distribution has also been analyzed for the lower tail of the cumulative distribution function (CDF). These parameters offer information about the narrowband channel behavior that is useful for a better knowledge of the propagation characteristics at 60 GHz.

1. Introduction

There is an increasing interest in using the unlicensed 60 GHz frequency band for commercial applications because of its capability to provide extremely high data rates beyond 5 Gbps over short distances [1–4].

The IEEE 802.15.3c task group (TG3c) has recently published the standard for the millimeter-wave- (mmW-) based alternative physical layer extension for IEEE802.15.3, that is, physical layer (PHY) and media access control layer (MAC) specifications. The IEEE 802.15.3c [5] is a standard in the 60 GHz band for wireless personal area networks (WPAN) devices in the named wireless gigabit ethernet. Simultaneously, the industry has created the consortium wireless gigabit alliance, commonly called WiGig [6], which is devoted to the development and promotion of wireless communications in the 60 GHz band. This band offers the following advantages: (i) huge and readily available spectrum allocation with 7 GHz in both USA and Japan and 9 GHz in Europe, (ii) dense deployment and high frequency reuse, and (iii) reduced size of devices due to the small wavelength [2]. The output power of 60 GHz devices is mainly limited to 10 mW due to regulations. Moreover, the free space losses in the 60 GHz band are considerably higher than those in the microwave band. Thus, the mmW WPAN devices will be designed to operate mainly in short-range line-of-sight (LOS) environments.

Since high data rates available in the IEEE 802.15.3c standard are achieved with multiple-input and multiple-output (MIMO) techniques [5], it is of paramount importance to characterize adequately the propagation channel in such band.

Several measurement campaigns have been carried out to model adequately the propagation channel at the 60 GHz band [7–15]. In [7], a stochastic channel model has been derived from measurements conducted in office, private house, library, and laboratory environments. The Triple-S and Valenzuela (TSV) statistical model has been proposed in [8] for the mmW band from the well-known Saleh and Valenzuela (SV) model. A modified SV model has been

derived in [9] where the deterministic two-path model is extended to a statistical two-path model by introducing random variables for the antenna position and merging with the conventional SV model which is suitable to express non-line-of-sight (NLOS) path components. In [10], power delay profiles (PDPs) and power angle profiles (PAPs) have been measured in various indoor and short-range outdoor environments. These experimental functions have been compared to results provided with image based on ray tracing techniques, by separating the multipath components (MPCs) in angle of arrival (AOA) and time of arrival (TOA). Measurements in a modern office block addressed to characterize the path loss were carried out in [11]. In [12], Smulders has reviewed the statistical description of an extensive number of measurements campaigns and channel modeling published previously.

As a result of some of such works, the TG3c channel modeling subcommittee released a report where a comprehensive channel model is presented based on measurements conducted in several environments [16].

The high speed interface (HSI) mode of the IEEE 802.15.3c standard is designed for devices with low-latency and bidirectional high-speed data and uses orthogonal frequency domain multiplexing (OFDM) [5]. Since the guard interval in the OFDM-HSI mode is higher than the root mean square (rms) delay spread in the majority of indoor environments [7, 10, 11], an accurate characterization of the narrowband channel is required for the 60 GHz frequency band.

Concretely, small-scale fading analyses in the 60 GHz have been addressed in some works to characterize the received amplitude [12–14]. In [13], the small-scale amplitude in LOS measurements conducted in three corridors of an office block with a bandwidth of 1 GHz was modeled as a Rice distribution. Values of mean and standard deviation of the Rice K-factor have been reported for two antenna types: an open-ended waveguide (OWG) and lens. The small-scale amplitude has been found to follow a Rayleigh distribution in an urban environment with ranges up to 400 m [14].

In spite of the numerous researches' efforts, an extensive study of the small-scale fading amplitude in the 60 GHz frequency band remains still open in the technical literature. Furthermore, the performance of MIMO techniques depends strongly on the multipath characteristics of the signal at the receiver device. Therefore, an exhaustive analysis of the fading phenomenon in the 60 GHz band is vital for the deployment of such systems.

In this paper, we will address an extensive study of the fading distribution in the 60 GHz band with LOS conditions from a measurement campaign carried out in a laboratory. The small-scale amplitude of the received signal is modeled as distributions proposed in the literature for modeling the fading amplitude: Rayleigh, Rice, Weibull, Nakagami-m, and α-μ distributions. Recently, several distributions have been proposed to model the small-scale fading in LOS condition [17, 18]. Nevertheless, to the best of the authors' knowledge, no estimators have been derived for the two-wave with diffuse power (TWDP) fading distribution proposed in [17]. In [18], the estimators of the κ-μ fading distribution

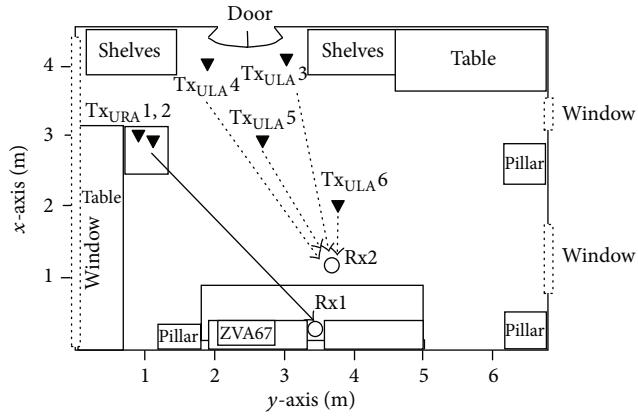

Figure 1: Map of measurements.

are calculated by using the method of moments with the moments of orders 4th and 6th. It is well known that the higher the order of moments used in the method of moments is, the poorest performance of such estimators is. Therefore, we have not analyzed both distributions in this paper. From experimental data, we have obtained the best-fit distribution and the distribution of the parameters inferred for Rayleigh, Rice, Weibull, Nakagami-m, and α-μ distributions.

This paper is organized as follows: firstly, the measurement campaign and the measuring setup are exposed in Section 2. In Section 3, the estimators of the distributions used to model the small-scale fading are presented. Next, Section 4 includes the results of the best-fitting distributions. Finally, the conclusions are discussed in Section 5.

2. Measurement Setup

Measurements have been performed in a laboratory of the Universidad Politécnica de Cartagena, Spain. The scenario consists of a room of dimensions approximately 4.5 × 7 × 3 m and it is furnished with several closets, desktops, and computers. The walls are made of plasterboard, whereas the floor is made of concrete. Figure 1 shows a top view of the room where measurements have been performed.

The channel sounder is based on the vector network analyzer (VNA) Rhode ZVA67, which has a dynamic range of 110 dB at 60 GHz. A resolution bandwidth of 10 Hz has been used and the band is 57–66 GHz. Both ports have V/1.85 mm female connectors. The antennas used in the measurements have a 5 dBi gain (manufacturer: Q-par 55 to 65 GHz omnidirectional antennas with V/1.85 mm type connector). A scheme of the channel sounder can be found in Figure 2.

The receiving antenna (Rx) is connected to the receiving port of the VNA using a 2 m coaxial cable, while the signal of the transmitting port of the VNA is twice amplified before being connected to the transmitter antenna (Tx), with a total length cable of 6.5 m (4 m + 2 m + 0.5 m). The reference of the two 25 dB amplifiers is HXI HLNA-465. The insertion losses of the cable are around 6 dB/m at 66 GHz. The polarization of antennas is vertical. For each combination of the Tx/Rx,

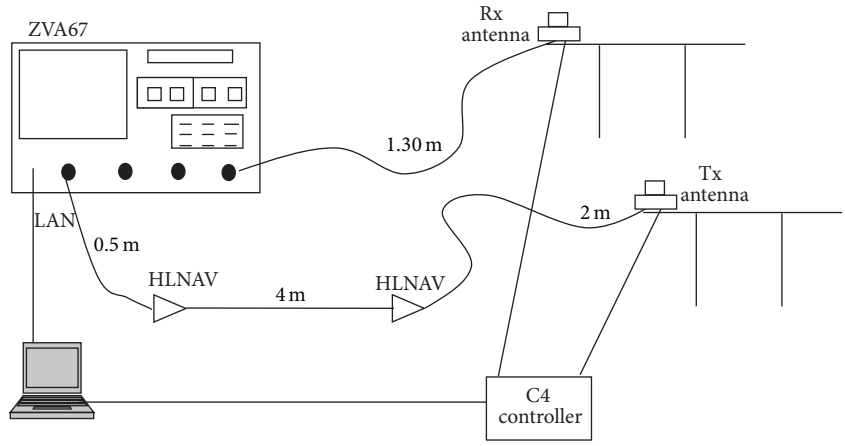

Figure 2: Scheme of the channel sounder.

we use virtual arrays by means of a linear positioning system moved by a C4 controller, and measurements can be distinguished into two groups.

Tx1-2 (corresponding to Rx1-2): in this case, the transmitter is placed in a bidimensional virtual array, uniform rectangular array (URA) 2D positioner, while the receiver uses a unique position.

Tx3-6 (corresponding to Rx3-6 each): both the transmitter and the receiver use uniform linear array (ULA).

The ULA are oriented in the y-axis corresponding to Figure 1. The URA are oriented in the x- and y-axes.

More details can be found in Table 1. The space between positions is 2 mm in both ULA and URA. The measurement process is controlled by a Matlab-based software executed from a laptop, which is connected to the VNA by a local area network (LAN) and to the C4 controller by a RS232 connection.

Each configuration has a bandwidth of 9 GHz and number of equal space frequency points, which are also summarized in Table 1. The transmitted power by the VNA was set to −10 dBm (in order not to saturate the first amplifier), giving a dynamic range of more than 100 dB at 66 GHz; that is, all of the cable attenuation is compensated by the two amplifiers and the measurement is calibrated using the through method. During the measurement process, nobody was in the room, so the channel can thus be considered as stationary. All of the measurement process has been carefully checked by analyzing the frequency response and by measuring the LOS component in the time domain. An analysis of the path-loss, correlation coefficients, and throughput in such scenario is carried out in [19].

3. Estimators of the Small-Scale Fading Distribution

In this section, estimators of the most employed distributions for small-scale modeling are described besides both the probability density functions (PDFs) and the cumulative distribution functions (CDFs). The Rayleigh, Rice, Weibull, Nakagami-m, and α-μ distributions can adequately characterize different fading conditions.

There are several methods to estimate parameters in distributions. The maximum likelihood estimation (MLE) is superior to the other estimation methods. Nevertheless, the derivation of MLE estimators cannot be straightforward [20]. For instance, a scalar nonlinear equation system is obtained in MLE method for the α-μ distribution without a single solution. The method of moments (MM) provides in many distributions consistent estimators and the estimating equations are simple in many situations [20]. For the α-μ distribution and Nakagami-m distributions, we have used the log-moments method, since it offers more superior performance than MM.

Let r be the instantaneous received field strength amplitude expressed in V/m. Thus, the received field strength in dBV/m is given by $\varepsilon = A \ln r$, where

$$A = \frac{20}{\ln 10}. \tag{1}$$

From the measurements records, we assume a sample size of N. Thus, $r_i, \varepsilon_i,\ i = 1, \ldots, N$ correspond to each observation in linear and logarithmic units, respectively. The sample nth raw moments of r and ε are defined as

$$\widehat{\mu}'_{r_n} = \frac{1}{N}\sum_{i=1}^{N} r_i^n, \tag{2}$$

$$\widehat{\mu}'_{\varepsilon_n} = \frac{1}{N}\sum_{i=1}^{N} \varepsilon_i^n, \tag{3}$$

respectively. We can calculate the sample nth central moments of r and ε as

$$\widehat{\mu}_{r_n} = \frac{1}{N}\sum_{i=1}^{N}\left(r_i - \widehat{\mu}'_{r_1}\right)^n, \tag{4}$$

$$\widehat{\mu}_{\varepsilon_n} = \frac{1}{N}\sum_{i=1}^{N}\left(\varepsilon_i - \widehat{\mu}'_{\varepsilon_1}\right)^n. \tag{5}$$

3.1. Rayleigh Distribution. If both the inphase and quadrature components of the complex baseband received signal follow a Gaussian distribution with 0 mean and standard deviation σ, then the amplitude of the received signal r, is a Rayleigh random variable (RV). This situation frequently occurs in the NLOS case, where the real and imaginary parts of the MPC fulfill these conditions since they are composed of the sum of a large number of waves. Thus, the sum of enough independent RVs provided the fact that no one of the RV dominates very closely to a normal distribution [21]. Nevertheless, the Rayleigh distribution has been extensively used to model the small-scale received amplitude in several environments due to its simplicity.

Assuming that r follows a Rayleigh distribution, the PDF of r is given by

$$p(r) = \frac{r}{\sigma^2} \exp\left(-\frac{r^2}{2\sigma^2}\right), \quad r \geq 0, \tag{6}$$

where $\sigma = \sqrt{E[r^2]/2}$, denoting $E[\cdot]$ expectation.

Likewise, the PDF of ε can be written as

$$p(\varepsilon) = \frac{1}{A\sigma^2} \exp\left(\frac{2\varepsilon}{A} - \frac{e^{2\varepsilon/A}}{2\sigma^2}\right), \quad -\infty < \varepsilon < \infty, \tag{7}$$

where A is given by (1).

The CDF in linear and logarithm units are given by

$$F(r) = 1 - \exp\left(-\frac{r^2}{2\sigma^2}\right), \quad r \geq 0, \tag{8}$$

$$F(\varepsilon) = 1 - \exp\left(-\frac{e^{2\varepsilon/A}}{2\sigma^2}\right), \quad -\infty < \varepsilon < \infty, \tag{9}$$

respectively.

Using the MLE method, σ can be estimated from the samples r_i, $i = 1, \ldots, N$ as

$$\widehat{\sigma} = \sqrt{\frac{1}{2}\widehat{\mu}'_{r_2}}. \tag{10}$$

3.2. Rice Distribution. In LOS situations, very often the received signal is composed of random MPCs, whose amplitude is described by the Rayleigh distribution plus a coherent LOS component which has essentially constant power. The power of this component, denoted by ν^2, is frequently higher than the total multipath power, symbolized as $2\sigma^2$.

Hence, the PDF of a Rice distribution can be expressed as

$$p(r) = \frac{r}{\sigma^2} \exp\left(-\frac{r^2 + \nu^2}{2\sigma^2}\right) I_0\left(\frac{\nu r}{\sigma^2}\right), \quad r \geq 0, \tag{11}$$

where $I_a(\cdot)$ is the modified Bessel function of the first kind with order a[22, 8.406].

The Rice factor, K, extensively used in radio propagation is defined as

$$K = \frac{\nu^2}{2\sigma^2}, \tag{12}$$

which represents the ratio between power of the coherent LOS component and the power in the other scattered MPCs.

The PDF of ε is expressed as

$$p(\varepsilon) = \frac{1}{A\sigma^2} \exp\left(\frac{2\varepsilon}{A} - \frac{e^{2\varepsilon/A} + \nu^2}{2\sigma^2}\right) I_0\left(\frac{\nu e^{\varepsilon/A}}{\sigma^2}\right), \quad -\infty < \varepsilon < \infty, \tag{13}$$

where A is given by (1).

The CDF of r and ε can be written as

$$F(r) = 1 - Q\left(\frac{\nu}{\sigma}, \frac{r}{\sigma}\right), \quad r \geq 0, \tag{14}$$

$$F(\varepsilon) = 1 - Q\left(\frac{\nu}{\sigma}, \frac{\exp(2\varepsilon/A)}{\sigma}\right), \quad -\infty < \varepsilon < \infty, \tag{15}$$

respectively, where $Q(a, b) = \int_b^\infty x \exp(-(x^2+a^2)/2) I_0(ax) dx$ is the Marcum Q function [23].

In [24], an efficient algorithm to estimate the υ and σ parameters of the Rice distribution with the MM has been derived using the sample mean and the sample standard deviation. This recursive algorithm defines the function

$$g(\theta) = \sqrt{\xi(\theta)(1 + r^2) - 2}, \tag{16}$$

where

$$\xi(\theta) = 2 + \theta^2 - \frac{\pi}{8} \exp\left(-\frac{\theta^2}{2}\right) \left[\left(2 + \theta^2\right) I_0\left(\frac{\theta^2}{4}\right) + \theta^2 I_1\left(\frac{\theta^2}{4}\right)\right]^2, \tag{17}$$

$$r = \frac{\widehat{\mu}'_{r_1}}{\widehat{\mu}_{r_2}}.$$

From a starting point of iteration $\theta_0 > 0$, we recursively evaluate $g^m(\theta_0) = \underbrace{g(g(\cdots g(\theta_0)))}_{m \text{ times}}$ until $|g^i(\theta_0) - \theta_{i-1}| \leq \Delta$, where Δ is the required accuracy. From this point, the parameters of the Rice distribution can be calculated as

$$\widehat{\sigma} = \sqrt{\frac{\widehat{\mu}_{r_2}}{\xi(\theta_i)}}, \tag{18}$$

$$\widehat{\nu} = \sqrt{\widehat{\mu}'^2_{r_1} + \left(\xi(\theta_i) - 2\right)\widehat{\sigma}^2}, \tag{19}$$

where $\theta_i = g^i(\theta_0)$ has been obtained in the ith iteration. Note that the minimum theoretical value of r is $\sqrt{\pi/(4-\pi)}$ that corresponds to a Rayleigh distribution; that is, $\upsilon = 0$. Hence, if $r < \sqrt{\pi/(4-\pi)}$, then υ is fixed to 0, and from (11) the estimated distribution becomes Rayleigh.

3.3. Nakagami-m Distribution. In several environments, the Rayleigh and Rice distributions cannot characterize satisfactorily the behavior of the received signal amplitude. For

instance, if two paths are of comparable power and are stronger than all the others, the amplitude signal does not fit neither Rice nor Rayleigh distributions.

The Nakagami-m distribution [25] assumes that the received signal is a sum of vectors with random magnitude and random phases with less restriction than both the Rice and Rayleigh distributions, thus providing more accuracy in matching experimental data than the use of such distributions [26].

The PDF of the Nakagami-m distribution in linear and logarithmic units is given by

$$p_r(r) = \frac{2}{\Gamma(m)}\left(\frac{m}{\Omega}\right)^m r^{2m-1}\exp\left(-\frac{mr^2}{\Omega}\right), \quad r \geq 0, \quad m > \frac{1}{2},$$
$$p_\varepsilon(\varepsilon) = \frac{2}{A\Gamma(m)}\left(\frac{m}{\Omega}\right)^m \exp\left(\frac{2m\varepsilon}{A} - \frac{me^{2\varepsilon/A}}{\Omega}\right), \quad -\infty < \varepsilon < \infty, \tag{20}$$

where A is given by (1), $\Omega = E[r^2]$, $\Gamma(\cdot)$ is the gamma function [22, (8.310)], and $m = \Omega^2/\mathrm{var}(r^2)$ is the fading parameter which provides information about the severity of fading, being var$(\cdot)$ the variance operator. For $m = 1$, the Nakagami-m becomes a Rayleigh distribution. Compound small-scale fading and shadowing amplitudes can be modeled with Nakagami-m distributions with $1/2 < m < 1$. That is why the standard deviation of the logarithmic amplitude distribution exceeds the maximum theoretical value for a small-scale distribution of 5.57 dB which corresponds to the Rayleigh fading distribution ($m = 1$). Note that the smaller fading parameter, m, the higher standard deviation of the log distribution. If we assume that the small-scale and shadowing distribution are independent processes, the variance of the log composite distribution is the sum of the variance of the log small-scale and the log shadowing distributions.

We can easily calculate the CDF of the Nakagami-m in linear and logarithmic units as

$$F_r(r) = \frac{\gamma\left(m, (m/\Omega)\, r^2\right)}{\Gamma(m)}, \quad r \geq 0, \tag{21}$$

$$F_\varepsilon(\varepsilon) = \frac{\gamma\left(m, (m/\Omega)\exp(2\varepsilon/A)\right)}{\Gamma(m)}, \quad -\infty < \varepsilon < \infty, \tag{22}$$

where $\gamma(a, b) = \int_0^b t^{a-1}\exp(-t)dt$ is the lower incomplete gamma function [22, (8.350)].

In [27, 28], an approximation of the log-moments method for m was derived as

$$\widehat{m} = \frac{4.4}{\sqrt{\widehat{\mu}_{\varepsilon_2}}} + \frac{17.4}{\widehat{\mu}_{\varepsilon_2}^{1.29}}, \quad \widehat{\Omega} = \widehat{\mu}'_{r_2}, \tag{23}$$

where $\widehat{\mu}'_{r_2}$ and $\widehat{\mu}_{\varepsilon_2}$ are the second sample raw moment of r given by (2) and the second sample central moment of ε given by (3), respectively.

3.4. Weibull Distribution. The Weibull distribution has been used to model fading amplitudes mainly in indoor environments [29, 30] where the separation of the small-scale and long-term fading is frequently cumbersome and this distribution can fit well the measurements.

The PDF of the Weibull distribution in both linear and logarithmic units is given by

$$p_r(r) = \frac{\alpha r^{\alpha-1}}{\Omega^\alpha}\exp\left(-\frac{r^\alpha}{\Omega^\alpha}\right), \quad r \geq 0,\ \alpha > 0, \tag{24}$$

$$p_\varepsilon(\varepsilon) = \frac{1}{A}\frac{\alpha\varepsilon^{\alpha-1}}{\Omega^\alpha}\exp\left(\frac{\alpha}{A}\varepsilon - \frac{1}{\Omega^\alpha}e^{\alpha\varepsilon/A}\right), \quad -\infty < \varepsilon < \infty, \tag{25}$$

where A is given by (1) and α and Ω are the shape and scale parameters of the Weibull distribution, respectively.

From (24) and (25), we can easily obtain the CDF of the Weibull distribution in both linear and logarithmic units as

$$F_r(r) = 1 - \exp\left(-\frac{r^\alpha}{\Omega^\alpha}\right), \quad r \geq 0, \tag{26}$$

$$F_\varepsilon(\varepsilon) = 1 - \exp\left(-\frac{e^{(\alpha/A)\varepsilon}}{\Omega^\alpha}\right), \quad -\infty < \varepsilon < \infty. \tag{27}$$

The Weibull distribution turns into the Rayleigh distribution for $\alpha = 2$. Composite small-scale and shadowing distributions can be modeled as Weibull distributions with $0 < \alpha < 2$.

Combining the methods of log-moments and moments, we can easily estimate the parameters of the Weibull distribution as [30]

$$\widehat{\alpha} = \frac{A\pi}{\sqrt{6}}\frac{1}{\sqrt{\widehat{\mu}_{\varepsilon_2}}} = \frac{11.14}{\sqrt{\widehat{\mu}_{\varepsilon_2}}}, \quad \widehat{\Omega} = \frac{\widehat{\mu}'_{r_1}}{\Gamma\left(1 + \dfrac{1}{\alpha}\right)}, \tag{28}$$

where $\widehat{\mu}'_{r_1}$ and $\widehat{\mu}_{\varepsilon_2}$ are the first sample raw moment of r given by (2) and the second sample central moment of ε given by (3), respectively.

3.5. α-μ Distribution. Recently, in [31], Yacoub proposed the use of the α-μ or generalized gamma distribution to model the fading in nonlinear environments where the surfaces which cause diffuse scattering are correlated spatially. Nevertheless, this distribution had been employed previously in [32] to characterize shadowed channels, that is, composed long-term and small-scale fading effects. The main advantage of the α-μ distribution is its mathematical simplicity and versatility even though it includes important distributions as gamma, Nakagami-m, one-side Gaussian, and Rayleigh as particular cases.

The PDF of the α-μ distribution in linear units can be written as

$$p_r(r) = \frac{\alpha\mu^{\mu} r^{\alpha\mu-1}}{\Omega^{\alpha\mu}\Gamma(\mu)} \exp\left(-\mu\frac{r^{\alpha}}{\Omega^{\alpha}}\right), \quad r \geq 0, \quad \alpha > 0,\ \mu > 0, \tag{29}$$

where α is a parameter which controls the linearity, $\mu = E^2[r^{\alpha}]/\mathrm{var}(r^{\alpha})$, and $\Omega = \sqrt[\alpha]{E[r^{\alpha}]}$. For $\alpha = 2$, the α-μ distribution becomes a Nakagami-m distribution. If $\alpha = 2$ and $\mu = 1$, the α-μ distribution turns into a Rayleigh distribution. For $\mu = 1$, the α-μ distribution converts into a Weibull distribution.

From (29), the PDF of ε is obtained as

$$p_{\varepsilon}(\varepsilon) = \frac{1}{A}\frac{\alpha\mu^{\mu}\varepsilon^{\alpha\mu-1}}{\Omega^{\alpha\mu}\Gamma(\mu)} \exp\left(\frac{\alpha\mu}{A}\varepsilon - \frac{\mu}{\Omega^{\alpha}}e^{\alpha\varepsilon/A}\right), \quad -\infty < \varepsilon < \infty, \tag{30}$$

where A is given by (1).

We can calculate the CDF of r and ε as

$$F_r(r) = \frac{\gamma\left(\mu, (\mu/\Omega^{\alpha})\, r^{\alpha}\right)}{\Gamma(\mu)}, \quad r \geq 0, \tag{31}$$

$$F_{\varepsilon}(\varepsilon) = \frac{\gamma\left(\mu, (\mu/\Omega^{\alpha}) \exp\left((\alpha/A)\,\varepsilon\right)\right)}{\Gamma(\mu)}, \quad -\infty < \varepsilon < \infty. \tag{32}$$

In [33], an estimation of such parameters has been derived based on the log-moments method as

$$\widehat{\mu} = \begin{cases} \widehat{\eta}^2 + \dfrac{1}{2} & \widehat{\eta} \leq -2.85 \\ -0.0773\widehat{\eta}^4 - 0.6046\widehat{\eta}^3 - 0.7949\widehat{\eta}^2 & \\ \quad -2.4675\widehat{\eta} - 0.9208 & -2.85 < \widehat{\eta} \leq -0.6 \\ -132.8995\widehat{\eta}^3 - 232.0659\widehat{\eta}^2 & \\ \quad -137.6303\widehat{\eta} - 27.3616 & -0.6 < \widehat{\eta} < -0.5, \end{cases} \tag{33}$$

$$\widehat{\alpha} = A\sqrt{\frac{\psi'(\widehat{\mu})}{\widehat{\mu}_{\varepsilon_2}}}, \tag{34}$$

$$\widehat{\Omega} = \sqrt[\alpha]{E[\widehat{r}^{\alpha}]}, \tag{35}$$

where

$$\widehat{\eta} = \frac{\widehat{\mu}_{\varepsilon_2}^{3/2}}{\widehat{\mu}_{\varepsilon_3}}, \qquad E[\widehat{r}^{\alpha}] = \frac{1}{N}\sum_{i=1}^{N} r_i^{\alpha}, \tag{36}$$

$\psi'(x) = \partial\psi(x)/\partial x = \partial^2 \ln\Gamma(x)/\partial x^2$ is the polygamma function of first order [34, (6.4.1)], and $\widehat{\mu}_{\varepsilon_2}$ and $\widehat{\mu}_{\varepsilon_3}$ are the sample central moments of second and third order of ε, calculated as (5).

4. Results

In this section, we present results of the fading amplitude distributions for the six measurements shown in Table 1 with positions depicted in Figure 1. Firstly, the main parameters of each measurement such as the coherence bandwidth, rms delay spread, and mean delay are calculated. Next, the statistical Kolmogorov-Smirnov (K-S) test is used to evaluate the goodness-of-fit of the above distributions, and finally we obtain the distribution of the most important estimators for such distributions. Finally, we have analyzed the matching of the estimated distributions in their lower tails to the experimental distribution.

4.1. Main Wideband Parameters. The principal wideband parameters for each measurement have been included in Table 2. Both mean excess delay and rms delay spread have been calculated from the measured power delay profile (PDP). To mitigate the noise effect on the rms derivation, we have considered a threshold level of 10 dB above the noise level floor. Since the rms delay spreads calculated for all the measurements are considerably smaller than 24.24 ns, which is the guard interval in the OFDM-HSI mode [5], the behavior of the PDP profile does not affect substantially the performance of this mode; that is, the intersymbol interference (ISI) is negligible.

The coherence bandwidth has been calculated for a high normalized frequency autocorrelation function value of 0.9; that is, $R_T(\Delta f) = 0.9$. The coherence bandwidths for all measurements are larger than the subcarrier spacing of 5.15625 MHz in the OFDM-HSI mode [5] except for the measurement #4, which is around 5 MHz. Therefore, we can also ignore the time dispersion effect on the system performance.

4.2. Best-Fit Distribution and Kolmogorov-Smirnov Test. Using the estimators detailed in Section 3, we have evaluated the inferred Rayleigh, Rice, Nakagami-m, Weibull, and α-μ distributions for each point of frequency in each measurement. These distributions are compared to the experimental distributions. To estimate the parameters of the Rice distribution, the accuracy parameter Δ is fixed to 10^{-8}.

In Figure 3, the PDFs of the above distributions in logarithmic units given by (7), (13), (25), (27), and (30) are plotted beside the experimental logarithmic PDF for the 2nd bin (frequency of 57.002 GHz) of the measurement #1. Note that the relationship between the received power in dBm, $\varepsilon_{\mathrm{dBm}}$, and the field strength in dBV/m, $\varepsilon_{\mathrm{dBV/m}}$, is given by

$$\varepsilon_{\mathrm{dBm}} = \varepsilon_{\mathrm{dBV/m}} + 10\log\left(\frac{\lambda^2}{480\pi^2}\right) + G_{\mathrm{dB}} + 30, \tag{37}$$

where λ is the wavelength and G_{dB} is the receiver antenna gain in dB.

The α-μ, Weibull, and Rice distributions match rather well the experimental distribution. In fact, the best-fit is the Weibull distribution in this case.

The statistical K-S test has been assessed for these distributions over all the bins of frequency in each measurement.

Table 1: Main parameters in each measurement experiment in the 57–66 GHz band.

Number of measurement	Tx—Rx	Number of points	Positions	Separation
1	1—1	4096	40 × 20 Tx; 1 Rx	3.79 m
2	2—1	10001	5 × 5 Tx; 1 Rx	3.84 m
3	3—2	8192	10 Tx; 10 Rx	3.40 m
4	4—2	8192	10 Tx; 10 Rx	3.70 m
5	5—2	8192	10 Tx; 10 Rx	2.20 m
6	6—2	2048	156 Tx; 8 Rx	1.24 m

Table 2: Wideband parameters in each measurement experiment.

Number of measurement	Mean excess delay (ns)	rms delay spread (ns)	Coherence bandwidth for $R_T = 0.9$ (MHz)
1	5.8	6.09	11.5
2	3.39	5.39	6.5
3	3.48	4.8	6
4	4.9	5.4	5
5	4.58	5.2	11
6	3.03	3.74	15

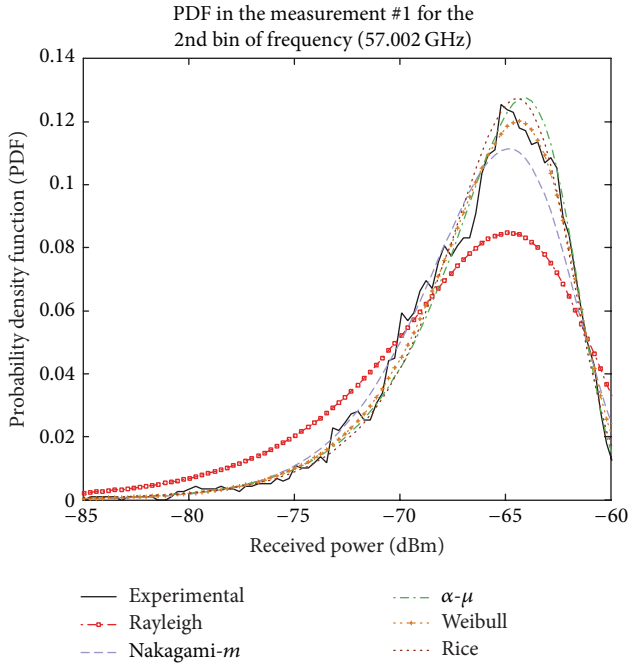

Figure 3: Probability density functions of the experimental, Rayleigh, Nakagami-m, α-μ, Weibull and, Rice distributions for the 2nd bin (frequency of 57.002 GHz) of the measurement #1.

The K-S confidence interval used is 5%. Moreover, we have calculated the best-fit distribution using the K-S test in each measurement. The best-fit distribution is calculated from the minimum value of

$$\max_{-\infty<\varepsilon_j<\infty} \left| F_{\varepsilon_{\text{experimental}}}(\varepsilon_j) - F_{\varepsilon_{\text{estimated}}}(\varepsilon_j) \right|, \tag{38}$$

where $F_{\varepsilon_{\text{experimental}}}(\varepsilon_j)$ is the experimental logarithmic CDF and $F_{\varepsilon_{\text{estimated}}}(\varepsilon_j)$ is the inferred logarithmic Rayleigh, Rice, Nakagami-m, Weibull, and α-μ CDFs given by (9), (15), (22), (27), and (32), both of them evaluated in ε_j.

Table 3 shows the percentage of the best-fist for the above distributions besides the K-S test accomplishment percentage over all the frequency bins in each measurement.

Note that the sum of the best-fit percentages for each measurement is 100%. In bold letters, we have highlighted the maximum best-fit distribution of each measurement. Since the measurements have been carried out in LOS condition, and in accordance with [13, 14], the Rice distribution is the most frequently best-fit distribution in the measurements from #1 to #5. In measurement #6, the Nakagami-m is the most frequently best-fit distribution even though the K-S test success of 90.5% for this distribution is less than the value of the percentage for the Rice distribution of 94.7%. Furthermore, the K-S test for the Rice distribution is fulfilled in at least 84.4% of frequency bins in the worst case, corresponding to the measurement #2. In measurements #3–#5, the K-S test percentage for the Rice distribution is very close to 100%.

4.3. Distribution of Estimated Parameters. Once the parameters of the Rayleigh, Rice, Nakagami-m, Weibull, and α-μ distributions are estimated from (10), (16)–(19), (23), (28), and (34)–(36), we can obtain the distribution of the main parameters of these distributions for each measurement.

Let γ_{P_2} and β_{P_2} be the skewness and kurtosis of the distribution of the parameter P defined as

$$\gamma_{P_2} = \frac{\mu_{P_3}}{\mu_{P_2}^{3/2}}, \qquad \beta_{P_2} = \frac{\mu_{P_4}}{\mu_{P_2}^{2}}, \tag{39}$$

respectively, where μ_{P_n} is the nth central moment of the distribution of P. The skewness is a measure of the asymmetry of the PDF of a real-valued RV whereas the kurtosis is an estimation of the "peakedness" of the PDF. A null skewness corresponds to a symmetrical PDF. A left-tailed PDF provides negative skewness and a positive skewness is obtained for right-tailed PDFs. Note that the skewness and kurtosis of a Gaussian distribution are equal to 0 and 3, respectively. We can also define the sample skewness, $\widehat{\gamma}_{P_2}$, and sample kurtosis, $\widehat{\beta}_{P_2}$, of the distribution of P in the same way of (2)–(5).

Table 3: Best-fit distributions percentages and Kolmogorov-Smirnov test accomplishment percentage for a confidence interval of 5%.

Number of measurement	1	2	3	4	5	6
α-μ						
K-S 5%	61	73.3	89.7	87.7	91	72.8
Best-fit	19.7	29	26.3	22.6	32.5	16.8
Rayleigh						
K-S 5%	4.4	6	42.7	59.8	15.1	0
Best-fit	0.3	1.4	1.1	1.8	0.2	0
Nakagami						
K-S 5%	71.3	66.4	98.3	97	98.7	**90.5**
Best-fit	23.6	17.6	15.9	12.7	19.1	**46.2**
Weibull						
K-S 5%	85.3	73.1	99.5	99.4	99.6	46.8
Best-fit	18	17	15.9	18	13.7	2.2
Rice						
K-S 5%	**91.9**	**84.4**	**99.9**	**100**	**99.9**	94.7
Best-fit	**38.4**	**35**	**40.9**	**45**	**34.4**	34.7

We have observed that the PDF of all the estimated parameters is highly right-skewed. That fact suggests that a lognormal distribution could approximate the distribution of some of these parameters. Therefore, we can evaluate the skewness and kurtosis of the distribution parameters expressed in dB.

Table 4 shows the sample log skewness, log kurtosis, sample mean, and sample standard deviation of the main estimated parameters of the Rice, Nakagami-m, Weibull, and α-μ distributions.

Following these results, both the fading parameter, m, of the Nakagami-m distribution and the shape parameter, α, of the Weibull distribution can be clearly modeled as a lognormal distribution. The Rice K-factor in dB could also fit a Gaussian distribution in measurements #3, #5, and #6. Nevertheless, both α and μ parameters of the α-μ distribution cannot be modeled as a lognormal distribution in spite of the PDF symmetry due to the small sample skewness values. Figure 4 shows the PDF of the Rice K-factor in dB and the Gaussian approximation for the measurements #1 and #5. Since the skewness of both K-factor distributions are very close to 0, the experimental PDFs are symmetrical. In spite of the fact that the kurtosis of the K-factor distribution, which is equal to 4 in the measurement #1, is slightly different from the theoretical value for the Gaussian distribution that is 3, the appearance of experimental and estimated PDFs is similar.

The mean of the K-Rice parameter oscillates from 3.21 to 8.45 dB. The values of the K-Rice parameter mean are equal to or higher than 4 dB except for the measurement #4. Note that the separation between Tx and Rx in the measurement #4 is the highest of all the experiments and the scatterers are closer to the Rx than the rest of the measurements.

The mean of the Rice K-factor can be related to the mean of the fading parameter, m, of the Nakagami-m distribution following the method of moments as follows [35]:

$$m = \frac{(1+K)^2}{1+2K}. \quad (40)$$

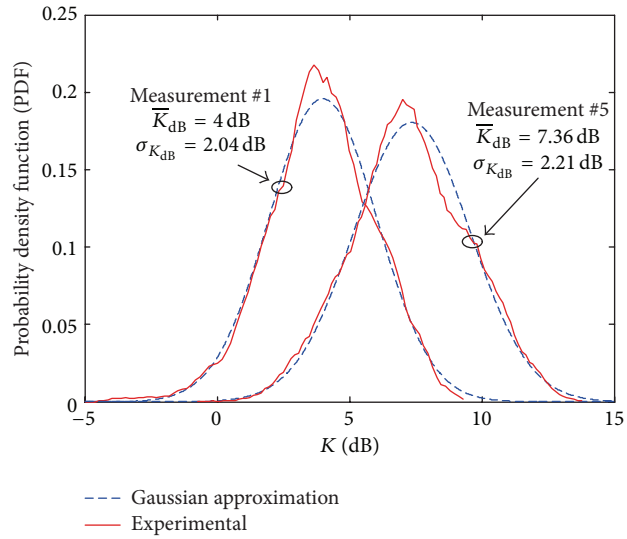

Figure 4: Probability density functions of the Rice K-factor in dB and the Gaussian approximation for the measurements #1 and #5.

From (40), the smaller Rice K parameter is, the lower fading parameter, m, is for $m \geq 1$. Mean fading parameters vary from 1.54 to 3.87. The standard deviation of the fading parameter is low with a maximum value of 2.06 for the measurement #2. We can compare $\overline{m}$, defined as the sample mean of the estimated fading parameter with the log-moments method (see Table 4), to $\overline{m}_{\text{Rice}}$, calculated from the sample mean of the estimated Rice K-factors using (40). Table 5 shows both parameters and the mean of the estimated Rice K parameter in both linear and logarithmic units.

From Table 5, it can be observed that $\overline{m}$ and $\overline{m}_{\text{Rice}}$ values are similar with a maximum difference between them of 0.4 for the measurement #6.

Table 4: Sample mean, standard deviation, log skewness, and log kurtosis of the main parameters of the estimated distributions.

Number of measurement	1	2	3	4	5	6
Rice						
K_{dB}						
Skewness	−0.4	−0.53	−0.2	−0.8	−0.1	−0.7
Kurtosis	4	4.33	3.59	5.88	2.73	3.82
Mean (dB)	4	5.46	4.97	3.21	7.36	8.45
St. dev. (dB)	2.04	3.1	3.01	2.23	2.21	1.68
Nakagami						
m						
L. skew.	0.53	0.46	0.65	0.52	0.24	−0.4
L. kurtosis	3.24	3.46	2.88	3.24	2.71	3.06
Mean	1.71	2.52	2.27	1.54	3.28	3.87
St. dev.	0.53	2.06	1.32	0.45	1.61	1.3
Weibull						
α						
L. skew.	0.55	0.15	0.43	0.33	0.01	−0.6
L. kurtosis	2.94	2.78	2.53	3.01	2.63	3.36
Mean	2.88	3.53	3.35	2.7	4.23	4.71
St. dev.	0.55	1.2	1.08	0.51	1.13	0.9
α-μ						
α						
L. skew.	1.05	0.54	0.81	0.84	0.62	2.1
L. kurtosis	3.96	5.36	4.69	3.47	5.3	10.4
Mean	5.58	4.31	4.73	4.97	4.72	4.34
St. dev.	5.22	5.81	5.58	5.27	6.07	3.71
μ						
L. skew.	−0.3	0.61	0.33	−0.2	0.41	−0.8
L. kurtosis	3.84	6.45	6.13	4.48	5.95	5.34
Mean	0.86	23.22	15.7	2.41	10.3	1.78
St. dev.	1.02	$1.2 \cdot 10^3$	875	72.4	186	1.37

Table 5: Sample mean of the Rice K-factor in logarithmic units and linear units. Sample mean of the fading parameter and mean of fading parameter calculated from the Rice K-factor.

Number of measurement			1	2	3	4	5	6
Rice	$\overline{K}_{\mathrm{dB}}$	Mean (dB)	4	5.46	4.97	3.21	7.36	8.45
	$\overline{K}$	Mean	2.51	3.51	3.14	2.09	5.44	6.99
Nakagami	$\overline{m}$	Mean	1.71	2.52	2.27	1.54	3.28	3.87
	$\overline{m}_{\mathrm{Rice}}$	Mean	2.05	2.54	2.35	1.85	3.49	4.27

Figure 5 shows the PDF of the fading parameter in dB, $10 \log m$, and the Gaussian approximation for the measurements #2 and #5. In spite of the fact that the kurtosis value of $10 \log m$ for the measurement #2 is not so different from 3, the difference between the experimental and the Gaussian PDFs is not negligible due to the significant value of skewness of 0.46 which provides a right-tailed or right-skewed experimental PDF. Similar conclusion can be extracted for the fading parameter distribution of the measurement #5.

The mean of the shape parameter, α, of the Weibull distribution oscillates from 2.7 to 4.71. On the one hand, the distribution is very different from the Rayleigh distribution since the mean of α is substantially higher than 2. On the other hand, the long-term fading is negligible in our measurements, since the standard deviation of the distribution in logarithmic units is considerably smaller than 5.57 dB which is the value for the log Rayleigh distribution ($\alpha = 2$). The higher α value of the Weibull distribution is, the smaller standard deviation of the logarithmic Weibull distribution is. A composite small-scale and log-term fading logarithmic distribution usually reaches a standard deviation that exceeds 5.57 dB which corresponds to estimated α values of the Weibull distribution lower than 2. The standard deviation of the α parameter of the Weibull distribution is low varying from 0.51 to 1.2. For the α-μ distribution, we have obtained considerably high standard deviations of the μ estimated parameter. Therefore,

Table 6: Mean and standard deviation of the difference between the relative received power of the estimated CDFs and the relative received power of the experimental CDF for the same value of the CDF, $p = 10^{-1}$, in the measurements #1 and #6.

Distribution		α-μ	Rayleigh	Nakagami	Weibull	Rice
Measurement #1	Mean (dB)	**0.088**	−3.12	−0.396	−0.16	0.135
	Standard deviation (dB)	**0.369**	1.137	0.34	0.315	0.368
Measurement #6	Mean (dB)	0.031	−4.39	−0.16	**−0.022**	0.053
	Standard deviation (dB)	0.228	0.861	0.1814	**0.1516**	0.1215

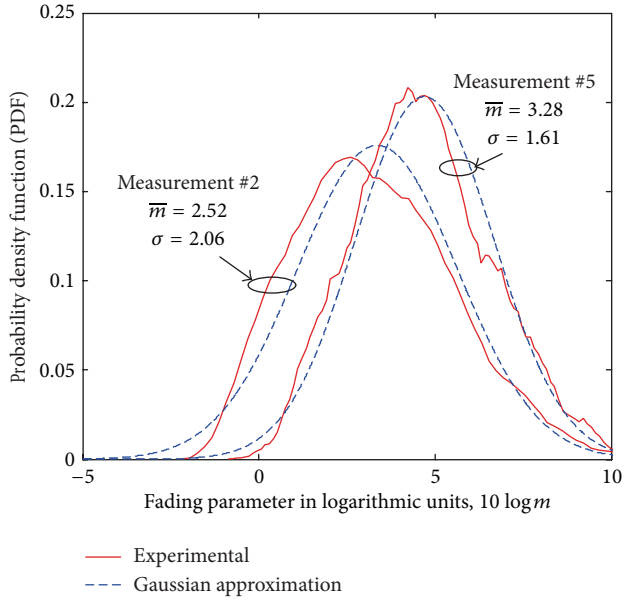

Figure 5: Probability density functions of the fading parameter in logarithmic units, $10 \log m$, and the Gaussian approximation for the measurements #2 and #5.

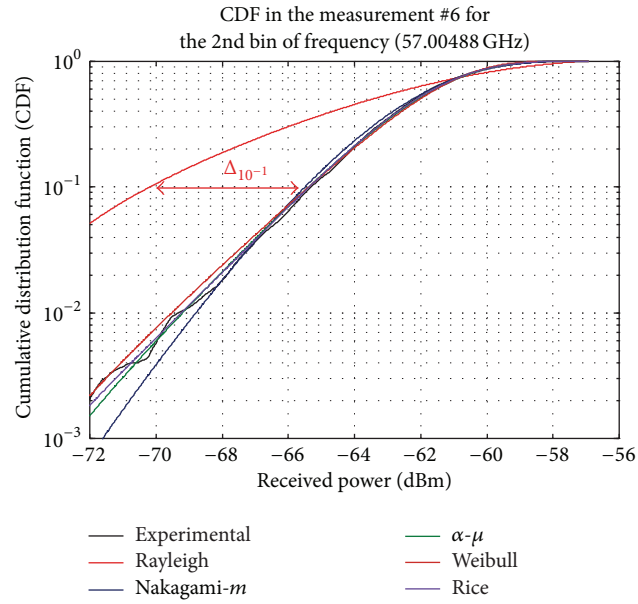

Figure 6: Cumulative distribution of the 2nd bin of frequency (57.00488 GHz) in the measurement #6. The difference between the relative received power of the estimated CDF and the relative received power of the experimental CDF for the same value of the CDF, $p = 10^{-1}$, is shown for the Rayleigh distribution.

the stability of this estimated parameter is substantially small. Nevertheless, the variation of the mean of the α estimated parameter for the α-μ distribution is not considerable since it oscillates from 4.31 to 5.58.

4.4. Lower Tail of the Distributions. In the analysis of performance in wireless communication systems, the lower tail of the distribution influences substantially the parameters, such as the outage probability, the bit error rate (BER), and the symbol error rate (SER), for high average signal-to-interference ratios. That is why the matching of the analytical distributions considered in this paper to the experimental distribution in the lower tails has been deeply analyzed in this subsection.

We have defined a relative received power, $\varepsilon_{\text{experimental}}$, for a given value of the experimental CDF, p, which can be written as

$$F_{\varepsilon_{\text{experimental}}}\left(\varepsilon_{\text{experimental}}\right) = p. \tag{41}$$

The relative received power for the Rayleigh, Rice, Nakagami-m, Weibull, or α-μ estimated CDFs, $\varepsilon_{\text{estimated}}$, for the same value of the CDF, p, is given by

$$F_{\varepsilon_{\text{estimated}}}\left(\varepsilon_{\text{estimated}}\right) = p. \tag{42}$$

Let Δ_p be the difference between the relative received power of the estimated CDF and the relative received power of the experimental CDF for the same value of the CDF, p, defined as

$$\Delta_p = \varepsilon_{\text{estimated}} - \varepsilon_{\text{experimental}}\Big|_p. \tag{43}$$

In Figure 6, $\Delta_{p=10^{-1}}$ is shown for the Rayleigh distribution in the measurement #6 and the 2nd bin of frequency (57.00488 GHz).

Since the number of samples of each observation is not high, we cannot calculate Δ_p for low values of p, provided that the experimental CDF is not stable for such low values as it can be observed in Figure 6. We can only evaluate this parameter for $p = 10^{-1}$ in the measurements #1 and #6, where the number of samples per record is significantly high.

In Table 6, the mean value $\Delta_{p=10^{-1}}$ and the standard deviation of $\Delta_{p=10^{-1}}$ are calculated for the measurements #1 and #6.

Surprisingly, the best-fit distribution for the low tails is not the same as the best-fit distribution using the K-S test for both measurements. In the measurement #1, the best-fit

distribution for the low tails is the α-μ instead of the Rice distribution obtained with the K-S test. In the same way, the best-fit distribution for the low tails is the Weibull instead of the Nakagami-m distribution calculated using the K-S test in the measurement #6.

5. Conclusions

In this work, an extensive study of the small-scale amplitude distribution in the 60 GHz band has been carried out for a LOS laboratory environment. Parameters of the Rayleigh, Rice, Nakagami-m, Weibull, and α-μ distributions have been estimated and such inferred distributions are compared to the experimental distribution using the Kolmogorov-Smirnov test. The Rice is the best-fit distribution followed by the α-μ and Nakagami-m distributions using the K-S test. However, the best-fit distributions for the low tails do not agree to the best-fit distributions obtained using the K-S test in the measurements #1 and #6. The K-S test for a confidence interval of 5% is fulfilled in over 84.4% of frequency bins for the Rice distribution in the worst-case experiment. From the calculation of the skewness and kurtosis of the logarithmic distribution, we have observed that both the Weibull shape parameter and the Nakagami-m fading parameter can be modeled as a lognormal distribution with small standard deviations, with maxima of 1.2 and 2.06, respectively.

Conflict of Interests

The authors declare that there is no conflict of interests regarding the publication of this paper.

Acknowledgments

This work was supported in part by the Spanish Ministerio de Ciencia e Innovación TEC-2010-20841-C04-1 and by the Universitat Politècnica de València, PAID 05-11 ref. 2702. The authors thank the anonymous reviewers for their valuable remarks and suggestions which have considerably enriched the final paper.

References

[1] P. Smulders, "Exploiting the 60 GHz band for local wireless multimedia access: prospects and future directions," *IEEE Communications Magazine*, vol. 40, no. 1, pp. 140–147, 2002.

[2] C. Park and T. S. Rappaport, "Short-range wireless communications for next-generation networks: UWB 60 GHz millimeter-wave wpan, and ZigBee," *IEEE Wireless Communications*, vol. 14, no. 4, pp. 70–78, 2007.

[3] R. C. Daniels and R. W. Heath Jr., "60 GHz wireless communications: emerging requirements and design recommendations," *IEEE Vehicular Technology Magazine*, vol. 2, no. 3, pp. 41–50, 2007.

[4] S. K. Yong, P. Xia, and A. Valdes-Garcia, *60 GHz Technology for Gbps WLAN and WPAN: From Theory to Practice*, Wiley, Chichester, UK, 2011.

[5] IEEE 802.15.3, *Wireless Medium Access Control (MAC) and Physical Layer (PHY) Specifications for High Rate Wireless Personal Area Networks (WPANs) Amendment 2: Millimeter-Wave-Based Alternative Physical Layer Extension*, IEEE, New York, NY, USA, 2009.

[6] WiGig White Paper: Defining the Future of Multi-Gigabit Wireless Communication, http://wilocity.com/resources/WiGigWhitepaper_FINAL5.pdf.

[7] T. Zwick, T. J. Beukema, and H. Nam, "Wideband channel sounder with measurements and model for the 60 GHz indoor radio channel," *IEEE Transactions on Vehicular Technology*, vol. 54, no. 4, pp. 1266–1277, 2005.

[8] H. Sawada, Y. Shoji, and C. Choi, "Proposal of novel statistic channel model for millimeter-wave WPAN," in *Proceedings of the Asia-Pacific Microwave Conference (APMC '06)*, pp. 1855–1858, Yokosuka, Japan, December 2006.

[9] Y. Shoji, H. Sawada, C.-S. Choi, and H. Ogawa, "A modified SV-model suitable for line-of-sight desktop usage of millimeter-wave WPAN systems," *IEEE Transactions on Antennas and Propagation*, vol. 57, no. 10, pp. 2940–2948, 2009.

[10] H. Xu, V. Kukshya, and T. S. Rappaport, "Spatial and temporal characteristics of 60-GHZ indoor channels," *IEEE Journal on Selected Areas in Communications*, vol. 20, no. 3, pp. 620–630, 2002.

[11] C. R. Anderson and T. S. Rappaport, "In-building wideband partition loss measurements at 2.5 and 60 GHz," *IEEE Transactions on Wireless Communications*, vol. 3, no. 3, pp. 922–928, 2004.

[12] P. F. M. Smulders, "Statistical characterization of 60-GHz indoor radio channels," *IEEE Transactions on Antennas and Propagation*, vol. 57, no. 10, pp. 2820–2829, 2009.

[13] H. J. Thomas, R. S. Cole, and G. L. Siqueira, "Experimental study of the propagation of 55 GHz millimeter waves in an urban mobile radio environment," *IEEE Transactions on Vehicular Technology*, vol. 43, no. 1, pp. 140–146, 1994.

[14] M. Choi, G. Grosskopf, and D. Rohde, "Statistical characteristics of 60 GHz wideband indoor propagation channel," in *Proceedings of the IEEE 16th International Symposium on Personal, Indoor and Mobile Radio Communications (PIMRC '05)*, vol. 1, pp. 599–603, September 2005.

[15] M. Kyrö, K. Haneda, J. Simola, K. Takizawa, H. Hagiwara, and P. Vainikainen, "Statistical channel models for 60 GHz radio propagation in hospital environments," *IEEE Transactions on Antennas and Propagation*, vol. 60, no. 3, pp. 1569–1577, 2012.

[16] S. K. Yong et al., "TG3c channel modeling sub-committee final report," IEEE 802.15-07-584-01, 2007.

[17] G. D. Durgin, T. S. Rappaport, and D. A. De Wolf, "New analytical models and probability density functions for fading in wireless communications," *IEEE Transactions on Communications*, vol. 50, no. 6, pp. 1005–1015, 2002.

[18] M. D. Yacoub, "The κ-μ distribution and the η-μ distribution," *IEEE Antennas and Propagation Magazine*, vol. 49, no. 1, pp. 68–81, 2007.

[19] M.-T. Martinez-Ingles, C. Sanchis-Borras, J.-M. Molina-Garcia-Pardo, J.-V. Rodriguez, and L. Juan-Llácer, "Experimental evaluation of an indoor MIMO-OFDM system at 60 GHz based on the IEEE802.15.3c standard," *IEEE Antennas and Wireless Propagation Letters*, vol. 12, pp. 1562–1565, 2013.

[20] K. D. Rao, *Linear Statistical Inference and Its Applications*, John Wiley & Sons, New York, NY, USA, 2nd edition, 1973.

[21] J. G. Proakis, *Digital Communications*, McGraw-Hill, Singapore, 3rd edition, 1995.

[22] I. S. Gradshteyn and I. M. Ryzhik, *Table of Integrals, Series and Products*, Academic Press, San Diego, Calif, USA, 7th edition, 2007.

[23] J. I. Marcum, *Table of Q Functions, U.S. Air Force RAND Research Memorandum M-339*, Rand Corporation, Santa Monica, Calif, USA, 1950.

[24] C. G. Koay and P. J. Basser, "Analytically exact correction scheme for signal extraction from noisy magnitude MR signals," *Journal of Magnetic Resonance*, vol. 179, no. 2, pp. 317–322, 2006.

[25] M. Nakagami, "The *m*-distribution—a general formula of intensity distribution of rapid fading," in *Statistical Methods of Radio Wave Propagation*, W. G. Hoffman, Ed., Pergamon Press, Oxford, UK, 1960.

[26] U. Charash, "Reception through nakagami fading multipath channels with random delays," *IEEE Transactions on Communications*, vol. 27, no. 4, pp. 657–670, 1979.

[27] R. W. Lorenz, "Theoretical distribution functions of multipath propagation and their parameters for mobile radio communication in quasi-smooth terrain," in *AGARD Terrain Profiles and Contours in Electromagnetic Wave Propagation*, SAO/NASA ADS, 1979.

[28] J. D. Parsons, *The Mobile Radio Propagation Channel*, John Wiley & Sons, New York, NY, USA, 2nd edition, 2000.

[29] H. Hashemi, "Indoor radio propagation channel," *Proceedings of the IEEE*, vol. 81, no. 7, pp. 943–968, 1993.

[30] R. Ganesh and K. Pahlavan, "On the modeling of fading multipath indoor radio channels," in *Proceedings of the IEEE Global Telecommunications Conference & Exhibition (GLOBECOM '89)*, vol. 3, pp. 1346–1350, November 1989.

[31] M. D. Yacoub, "The α-μ distribution: a physical fading model for the Stacy distribution," *IEEE Transactions on Vehicular Technology*, vol. 56, no. 1, pp. 27–34, 2007.

[32] A. J. Coulson, A. G. Williamson, and R. G. Vaughan, "Improved fading distribution for mobile radio," *IEE Proceedings—Communications*, vol. 145, pp. 197–202, 1998.

[33] J. Reig and L. Rubio, "On simple estimators of the α-μ fading distribution," *IEEE Transactions on Communications*, vol. 59, no. 12, pp. 3254–3258, 2011.

[34] M. Abramowitz and I. Stegun, *Handbook of Mathematical Functions*, National Bureau of Standards, Washington, DC, USA, 10th edition, 1972.

[35] M. K. Simon and M.-S. Alouini, *Digital Communications over Fading Channels*, John Wiley & Sons, New York, NY, USA, 2nd edition, 2005.